Electric control of spin-Hall effect by inter-valley transitions

N. Okamoto,[1] H. Kurebayashi,[2,1,3,*] T. Trypiniotis,[1,4] I. Farrer,[1] D. A. Ritchie,[1] E. Saitoh,[5,6,7] J. Sinova,[8,9] J. Mašek,[10] T. Jungwirth,[9,11] and C. H. W. Barnes[1]

[1]*Cavendish Laboratory, University of Cambridge, J. J. Thomson Avenue, Cambridge CB3 0HE, United Kingdom*

[2]*London Centre for Nanotechnology, UCL, 17-19 Gordon Street, WC1H 0AH, United Kingdom*

[3]*PRESTO, Japan Science and Technology Agency, Kawaguchi 332-0012, Japan*

[4]*Department of Physics, University of Cyprus, 1678 Nicosia, Cyprus*

[5]*Institute for Materials Research, Tohoku University, Sendai 980-8577, Japan*

[6]*The Advanced Science Research Center, Japan Atomic Energy Agency, Tokai 319-1195, Japan*

[7]*CREST, Japan Science and Technology Agency, Sanbancho, Tokyo 102-0075, Japan*

[8]*Institut fur Physik, Johannes Gutenberg-Universitat Mainz, 55128 Mainz, Germany*

[9]*Institute of Physics ASCR v.v.i., Cukrovarnická 10, 162 53 Praha 6, Czech Republic*

[10]*Institute of Physics ASCR v.v.i., Na Slovance 2, 182 21 Praha 8, Czech Republic*

[11]*School of Physics and Astronomy, University of Nottingham, Nottingham NG7 2RD, United Kingdom*

Abstract

Controlling spin-related material properties by electronic means is a key step towards future spintronic technologies. The spin-Hall effect (SHE) has become increasingly important for generating, detecting, and utilizing spin currents, but its strength - quantified in terms of the SHE angle - is ultimately fixed by the magnitude of the spin-orbit coupling (SOC) present for any given material system. However, if the electrons generating the SHE can be controlled by populating different areas (valleys) of the electronic structure with different SOC characteristic the SHE angle can be tuned directly within a single sample. Here we report the manipulation of the SHE in bulk GaAs at room temperature by means of an electrical inter-valley transition induced in the conduction band. The spin-Hall angle was determined by measuring an electromotive force driven by photo-excited spin-polarized electrons drifting through GaAs Hall bars. By controlling electron populations in different (Γ and L) valleys, we manipulated the angle from 0.0005 to 0.02. This change by a factor of 40 is unprecedented in GaAs and the highest value achieved is comparable to that of heavy metal Pt.

After its experimental discovery[1,2] led by theoretical predictions[3–6], the SHE has been used as an electric means of generating and probing spin currents in the field of spintronics[7]. The SHE arises from the relativistic SOC in the solid-state environment, by inducing a spin-dependent deflection perpendicular to the motion of the electron, which generates a spin-current from charge flow. Alternatively the reciprocal process converts a spin current into a charge current, termed the inverse SHE[8–11]. The strength of the SHE is characterized by the SH angle ($\theta_{\rm SH}$). In GaAs, a model material for SHE studies as it facilitates its direct optical detection[1,2], $\theta_{\rm SH}$ ranges within the order of 10^{-3} to 10^{-4} for n-doping depending on the carrier density and other material parameters[1,12,13]. In metals, the light element Al exhibits $\theta_{\rm SH} \sim 10^{-4}$ (Ref.8) whereas among heavy metals Pt shows $\theta_{\rm SH} \sim 0.004$-$0.08$[14] and Au has $\theta_{\rm SH} = 0.0035$[15]. Very recently, Ta with β-phase structure has been reported to have a very large SH angle, ($\theta_{\rm SH} = 0.2$)[16], which makes it relevant for generating spin-currents strong enough for MRAM technology based on spin-transfer torque with in-plane current geometries. Although there is much attention to exploring large SH angle materials[17–19], the *in-situ* electric control of the $\theta_{\rm SH}$ has not been reported. Attaining this electrical tunability offers new functional possibilities for future spintronics devices. The SH angle is determined by the electronic band structure and impurity states, which are weakly susceptible to an external electric excitation. The electric field however can induce carrier redistribution within a band or even between multiple bands. Particularly, the electric-field dependent inter-band transition is able to significantly change carrier charge transport by the valley degree of freedom, which is commonly used in semiconductor technology, e.g. in the Gunn diode[20]. In III-V semiconductors, two (L and X) satellite valleys exist other than the Γ valley, all of which have unique characters in terms of the transport property, different SOC and therefore different SHE signals. However, there is no report on SHE in the satellite valleys, nor report on how the inter-valley transition modifies the spin-Hall property of materials.

Here we present the room-temperature electric control of $\theta_{\rm SH}$ in bulk GaAs by the valley degree of freedom. We find that $\theta_{\rm SH}$ changes from 0.0005 to 0.02, a factor of 40, by the applied longitudinal electric field which facilitates the Γ-L inter-valley transition as a result of nonlinear electron transport. We use optical spin orientation techniques[21] to generate spin-polarized electrons in GaAs, which drift through our Hall-bar device and experience spin-dependent transverse deflection generating the inverse SHE (see Fig. 1a,b)[22–25]. As a

consequence, charge accumulation is built, measurable as the transverse voltage (see Methods):

$$V_{\perp} = \theta_{\mathrm{SH}} \rho_{\mathrm{N}} w j_{||} P, \tag{1}$$

where ρ_{N},w, $j_{||}$ and P are the resistivity of the sample, the Hall bar width, the longitudinal charge current, and the carrier spin-polarization respectively. When the applied longitudinal electric field is sufficiently high, electrons can transfer to the neighboring L-valley[20] (see Fig. 1c). Using this mechanism, we studied spin-dependent transport, i.e. the spin relaxation time and θ_{SH}, while electrically controlling the valley populations. The L-valley has significantly stronger SOC than the Γ-valley due to its larger p-character arising from stronger hybridization with the p-bands at finite wave-vector. The relative strength of the SOC is estimated to be larger in the L-valley by a factor of 93 (see below) which is comparable to the dramatic electric-field induced increase of the SH angle that we observe.

Figure 2a shows charge transport characteristics of our n-type GaAs sample measured under light illumination. The curve departs from the Ohmic behavior, particularly showing a negative differential resistance between $E_{||}$=200 and 350 kV/m. This is the signature of the Γ-L inter-valley transition reflecting the large electron effective mass in L-valleys m_L=0.22m_0[26] (compared to Γ-valley m_Γ=0.067m_0[26]). As such the inter-valley transition decreases the total electrons mobility with $E_{||}$, leading to the negative differential resistance observed in Fig. 2a. From the data with standard carrier transport model with constant effective-mass approximation, the electron mobilities in the Γ- and L-valley (μ_Γ and μ_L) were estimated as 0.763±0.002 and 0.199±0.001 m^2/Vs respectively (see Supplementary Information). This multi-valley state can be described by the two current channel model: $J_{||} = (en_\Gamma\mu_\Gamma + en_L\mu_L)E_{||}$, with n_Γ (n_L) being the carrier density of the Γ (L) valleys that varies with $E_{||}$. Using these valley carrier densities, we define the electron transition probability from the Γ to L valleys as: $P_L = n_L/(n_\Gamma + n_L)$, shown in Fig. 2c. The curve reveals that in our experiments we are able to control P_L from 0 to 100%. It should be noted that the observed inter-valley transition occurs in lower electric fields than previously reported values without illumination[20,27]. We attribute this to electron detrapping induced by light illumination. In the doped samples the excited photo-carriers are a small fraction of the total electron density and the on-set of the transition is not strongly influenced by the laser intensity (see Supplementary Information for more details).

We now describe our optically-induced SHE voltage measurements with the inter-valley

transition. Circularly-polarized light incident on our Hall-bar devices perpendicular to the sample plane excites out-of-plane spin-polarized carriers, which accelerate under $E_{||}$ and generate the $V_{\perp}$ we measured (see Methods and Fig. 2d). In order to rule out spin-independent components, the transverse voltage measured for linearly polarized light was used to subtract as a background signal. In the low biases ($0 < E_{||} < 125$ kV/m) $V_{\perp}$ shows a slight change with $E_{||}$ whereas it grows up significantly in the higher biases. This steep increase concurs with the increase of P_L and the onset occurs approximately when $P_L \sim 0.3$. In order to translate $V_{\perp}$ into $\theta_{\rm SH}$ using Eq. (1), we deducted P by using the spin-density rate equation together with the spin life time obtained by the Hanle measurements for each $E_{||}$. The spin-density rate equation describes the time evolution of spin-density $n_{\rm s}$ (n_s is only due to the photo-carriers since in dark the carriers in the n-GaAs are unpolarized; see Methods). In the stead-state condition($dn_{\rm s}/dt = 0$), $P(=n_{\rm s}/n_{\rm e})$ is given by $GP_0\tau_{\rm s}/n_{\rm e}$, where G is the rate of photo-carrier generation, P_0 is the electron spin polarization at instant of photo-excitation, and $\tau_{\rm s}$ is the spin life time. We use the value of G=3.94×10^{24} cm$^{-3}s^{-1}$(see Methods) and assume $P_0 = 0.5$ for the analysis of n-GaAs[21]. Since the electric modulation of P_0 and G are negligibly small in our applied electric field region[28], $\tau_{\rm s}$ is the only variable to determine P. We therefore measured $\tau_{\rm s}$ by performing the Hanle measurement, the observation of spin signal dephasing by the external magnetic field perpendicular to the spin polarization direction[21]. In our case, we applied an external magnetic field $\mathbf{B}_{\rm ex}$ along the in-plane direction parallel to $\mathbf{E}_{||}$ as in Fig. 3a, while measuring $V_{\perp}$. Note that in this geometry we can avoid the normal Hall effect in our $V_{\perp}$. Figure 3b shows observed Hanle curves for various $E_{||}$. Each curve was fit by the standard Hanle model equation (see Methods) to clarify the $E_{||}$ dependence of $\tau_{\rm s}$ shown in Fig. 3c. The analysis model includes the electron g-factor which is known to be different for the Γ[29] and L[30] valleys and so the overall g-factor is changing during the inter-valley transition regime. Precise g-factor values for the multi-valley states are not readily accessible, in particular for electrons excited into higher energy states and its distribution. We therefore exploited a basic approach that starts with the known g-factors (which are for electrons in the bottom of conduction bands for each valley) and weight them by the number of two valley populations to find the averaged g-factor for our analysis (see Supplementary Information). For $E_{||}$=12.5 kV/m, where all the electrons are populated in the Γ-valley, the obtained $\tau_{\rm s}$ = 192 ±5 ps is comparable to previously reported values for GaAs with similar doping density and temperature[31]. In the region where the electron

velocity (as seen in $j_{||}$) increased with $E_{||}$(<150 kV/m) observed in Fig.2**a**, $\tau_{\rm s}$ monotonically decreased with $E_{||}$. This reduction can be attributed to the D'yakonov-Perel'(DP) spin relaxation mechanism for bulk n-GaAs[32] as follows. An applied electric field enhances the DP mechanism since the field redistributes electrons into higher **k** states, which results in the increase of spin precession rates. This mechanism can qualitatively explain the observed decrease in $\tau_{\rm s}$ within the low bias region. In the inter-valley transition region i.e. $E_{||}$ >150 kV/m, the reduction of $\tau_{\rm s}$ continues further, and these observed short spin relaxation times in the GaAs L valley agree well with a previous study with optical orientation techniques[33]. Tong et al.[34] also theoretically calculated the multi-valley spin relaxation in GaAs. In the multi-valley state, the L valleys capture high-k electrons from the Γ valleys, which stops the further increase of the DP spin relaxation rate. In addition, due to a large effective mass in the L valleys, L-valley electrons are less likely to drift into higher-k states than electrons in the Γ valleys. As a result, $\tau_{\rm s}$ has a weak dependence on $E_{||}$ in the inter-valley electron transition regime. With the observed $\tau_{\rm s}$ and rate equation, we obtained P as a function of $E_{||}$ in Fig. 3**c** inset.

Using P calculated from the experimental data and other parameters in Eq.(1), we obtained $E_{||}$ dependence of $\theta_{\rm SH}$, as plotted in Fig. 4a. In the lowest data point of $E_{||}$, i.e. 12.5 kV/m where most of the electrons populate the Γ-valley, $\theta_{\rm SH}$ is found to be 5×10^{-4}. Engel et al.[35] developed theory of the spin-Hall conductivity in a bulk transport regime: $\theta_{\rm SH} \approx 2\lambda_{\rm SO}/(a_{\rm B}^*)^2 - 2n_{\rm e}\lambda_{\rm SO}e^2/\hbar\sigma_{\rm e}$, where λ_{so}, α_B^* and $\sigma_{\rm e}$ are the spin-orbit coupling parameter, the effective Bohr radius of an ionized impurity and the conductivity, respectively. The first term is the contribution from skew scattering and the second from the side jump mechanism. Using the equation with a set of parameters: $\lambda_{\rm SO}$=5.26 Å^2,[35] $a_{\rm B}$=103 Å,[35] $n_{\rm e} = 1.28\times10^{16}{\rm cm}^{-3}$, and $\sigma_{\rm e} = 1.28\times10^{-3}\Omega^{-1}{\rm m}^{-1}$, we obtained $\sigma_{SH} = 0.92\ \Omega^{-1}m^{-1}$ and $\theta_{\rm SH} = 7.3\ \times10^{-4}$ which is in good agreement with our experimental value. Furthermore, there are experimental accounts of $\theta_{\rm SH}$ for similar doping densities (but for low temperature) by Garlid et al.[13]($\theta_{\rm SH} = 8.3\times10^{-4}$) and Matsuzaka et al.[12] ($\theta_{\rm SH} \sim 6\ \times10^{-4}$) for Γ-valley electrons in n-GaAs, both of which fall within the same order of magnitude of $\theta_{\rm SH}$ we measured. In Fig. 4a, a moderate increase in $\theta_{\rm SH}$ with $E_{||}$ is observed in the low electric field region ($E_{||}$ <150 kV/m). This can be phenomenologically explained by the enhancement of SOC strength caused by the intra-band excitation already discussed in the above DP mechanism part. In the inter-valley transition region ($E_{||}$ >150 kV/m), by contrast, $\theta_{\rm SH}$ significantly

increases with $E_{||}$ up to the value of 2×10^{-2} at 500 kV/m.; *i. e.* a factor of 40 compared to the low field value. This spin-Hall angle is an unprecedented value in GaAs and comparable to $\theta_{\rm SH}$ in Pt[14]. The high value of $\theta_{\rm SH}$ is directly associated with the L-valley electrons, as is evidenced by re-plotting $\theta_{\rm SH}$ against P_L in Fig. 4b, which suggests that the observed $\theta_{\rm SH}$ can be described by the linear combination of $\theta_{\rm SH}$ in Γ and L valleys. This indicates that the main cause of the increase is indeed the inter-valley transition, which we have shown here, is controllable by a simple external electric bias. We also note that the spin Gunn effect proposed by Qi et al.[36] is not relevant to our observation (see Supplementary Information). The valley related SH angle is expected to be proportional to the SOC energy scale of each valley. In the L-valley, microscopic tight-binding calculations indicate a p-character from the heavier element As sublattice of about 15 %.[37] This allows us to use the scale at the Γ point, $\sim$ 1 meV,[38,39] and to compare it to its weighted valence band value, 340 meV for GaAs at the Γ point where it is 55% As p-like. This yields an expected increase in SH angle of $\sim (0.15 \times 340\text{meV}/0.55)/1\text{meV} \sim 93$ (see Supplementary Material for more detailed analysis). This value, which should only be considered as semiquantitative, compares well with the observed increase of the spin Hall angle in the experiment.

In order to reproduce the observed effect in other samples, we examined a sample with un-doped GaAs (the structure: un-doped GaAs (1000 nm)/ AlAs optical barrier (100 nm) / undoped GaAs buffer (100 nm) / un-doped GaAs substrate) and the results are shown in Fig. 5. We found that the carrier transport can be modified by the light intensity $I_{\rm i}$ and the onset of the inter-valley transition varies with $I_{\rm i}$ (Fig.5**c** and more discussions in Supplementary Information). Accordingly the measured $V_\perp$ and other spin-dependent parameters such as $\tau_{\rm s}$ and $\theta_{\rm SH}$ are also $I_{\rm i}$-dependent. Same as the n-type sample, the applied electric field induced the increase of $\theta_{\rm SH}$ by the inter-valley transition for all $I_{\rm i}$(Fig.5**f**). $\theta_{\rm SH}$ for the Γ-valley electron ($E_{||} = 47.2$ kV/m) is one order of magnitude smaller than that of the n-type sample measured. This is consistent with other work[12] in which the reduction of the extrinsic mechanism induced by impurity spin-dependent scattering lowers the angle compared with n-doped GaAs. The most remarkable part of these measurements is that $\theta_{\rm SH}$ excellently scales with P_L for all the intensities measured, as shown in Fig. 5**f** inset. Furthermore, this increase in $\theta_{\rm SH}$ by a factor of $\sim$12 for $P_L \sim 0.4$ agrees very well in order of magnitude with the factor of 40 (for $P_L = 1$) observed in the n-doped sample. These are another unambiguous evidence that the inter-valley transition predominantly governs the electric

control of θ_{SH}.

To conclude, we show in this paper that an external electric bias can significantly modify materials' spin-Hall angles when the inter-valley transition occurs. In particular, we observe orders of magnitude change of the SH angle induced by the applied electric field and the highest SH angle we achieve by this mechanism in a common III-V semiconductor is comparable to that of Pt, which is widely used as an excellent spin current detector owing to the heavy metal nature. This suggests that the inter-valley transition is a promising, alternative approach in searching for a large spin-Hall angle material, rather than merely using materials with heavier elements. Current semiconductor growth technologies are capable of engineering the strength of SOC as well as the position of satellite valleys with respect to the Γ-valley position by substituting Ga or As with other elements[40]. In particular, systematic alloying with Al, which lowers the L-valley relative to the Γ-valley, should be a key pathway to fully exploit and test the observed physics. We therefore envisage that further material investigations will lead to discoveries of giant spin-Hall angle materials with the inter-valley transition operating at a lower electric field. The present study also highlights the importance of spin transport properties in the conduction band L-valley which applies not only to III-V semiconductors but also to group IV-semiconductors such as Ge[41,42]. In terms of device applications, the electric means of controlling the spin-Hall angle is readily feasible and offers electric tunability of the creation/detection efficiency of spin currents, with clear relevance for future memory and logic devices.

I. METHODS

A. Measurement

The sample structure used in this study is Si-doped (the initial electron density n_e^0=1.01×10^{16} cm^{-3}) n-GaAs (3.0 μm) / AlAs optical barrier (50 nm)/ un-doped GaAs buffer (50 nm), each layer was grown by molecular beam epitaxy on un-doped GaAs substrate, which was designed to absorb almost all photon in the top layer. The lateral dimension of the Hall bar is 0.18 mm in longitudinal, 1.08 mm in transverse direction and the bar width is 80 μm with alloyed Ohmic contacts of GePd[43]. The circularly polarized light ($h\nu$ =1.58 eV, the light intensity I_i=80 mW) was modulated by a photoelastic modulator at 50 kHz and was incident at the center of the Hall bar with the spot size of 75 μm. Under the light excitation the electron density n_e became 1.28×10^{16} cm^{-3} determined by Hall measurements. This number is used to calculate the total mobility μ (shown in Fig. 2(b)) using $j_{||} = en_e\mu E_{||}$ and a mobility for each valley has been determined (see Supplementary Information).We measured the 50 kHz component of the ISHE induced transverse voltage $V_\perp$ by means of lock-in detection. At the same time, the longitudinal current density $j_{||}$ (=$I_{||}/s$, $I_{||}$: the longitudinal current, s: the cross-sectional area of the bar) was measured to characterize the longitudinal carrier transport.

B. Spin Hall angle in Eq. (1)

The spin Hall angle, which due to Onsager relations determines both the direct and inverse spin Hall effects[10], is defined as $\theta_{SH} = \rho_{SH}/\rho_N \approx \sigma_{SH}/\sigma_N$[23,44]. Here ρ_{SH} and σ_{SH} are the spin-Hall resistivity and conductivity, respectively, and ρ_N and σ_N are the longitudinal resistivity and conductivity, respectively. The transverse electric field generated by the ISHE[44], $\mathbf{E}_\perp = \rho_{SH}(\mathbf{j}_s \times \sigma)$ where $\mathbf{j}_s$ is the spin current with the spin-polarization unit vector σ, can be then written as $\mathbf{E}_\perp = \theta_{SH}\rho_N(\mathbf{j}_s \times \sigma)$[44]. In our optical spin injection experiment the transverse spin-Hall voltage is not generated by a pure spin current but a current which is partially spin-polarized due to the photocurriers generated by the circularly polarized light. This experimental geometry, previously referred to as spin-injection Hall effect[23] and akin to the anomalous Hall effect in a partially spin-polarized ferromagnet, implies that the pure spin current $\mathbf{j}_s$ is replaced by $j_{||}P$ in the above expression for the transverse spin-Hall electric

field. Finally, Eq. (1) is obtained by replacing $E_\perp$ with $V_\perp/w$, where w as the width of the bar.

C. spin density equation and Hanle analysis

The spin density rate equation consists of the generation and dissipation rate terms of spin density $n_s(=(n_\uparrow - n_\downarrow)/n_e$, $n_\uparrow$: up-spin density, $n_\downarrow$: down-spin density): $\partial n_s/\partial t = GP_0 - n_s/\tau_s$. Here, P_0 is the initial spin polarization value, $G = \alpha n_p(1-R)/d\int_0^d e^{-\alpha z}dz$ is the rate of the optically generated electron density (α: the absorption coefficient, n_p: the irradiated photon density in unit time, R: the reflectance of the sample, z: the variable of thickness direction, d: the thickness of the sample), and τ_s is the spin life time which is defined as $1/\tau_s = 1/\tau + 1/\tau_s^r$, ($\tau$: the photo-electron life time, τ_s^r: the spin relaxation time). With each spin decay characteristic time, the time evolution of spins is given by: $S = S_0\exp(-t/\tau_i)$ where S_0, t are the initial spin number and time respectively, and τ_i is either τ_s or τ_s^r. For our Si-doped GaAs ($h\nu$ =1.58 eV, I_i=80 mW), we use α=1.5×10^4 cm^{-1} (Ref.45), n_p=1.79×10^{21} cm^{-2}, R=0.305 (Ref.45), t=3.0 μm, making G = 3.94×10^{24} cm^{-3}. In the equilibrium condition, n_s is given by $GP_0^l\tau_s$ and the spin polarization is $P = n_s/n_e = GP_0\tau_s/n_e$. τ_s was determined by our Hanle-type measurements using the following equation: $V_\perp(B_{ex}) = V_\perp(0)/\{1+(\Omega\tau_s)^2\}$ and $\Omega = \mu_B g_{eff} B_{ex}/\hbar$. Here μ_B is the Bohr magneton, and g_{eff} is the effective g-factor. (See Supplementary Information for a detailed discussion of the Hanle measurements.) Using experimentally-obtained τ_s and τ which can be calculated by the charge equilibrium condition (n=Gτ) and the photoexcited carrier density (n=2.8×10^{15}cm^{-3}) from the transport data, we found τ_s^r=263 ps with τ_s=192 ps and τ=711 ps. Therefore, τ_s^r and τ are within the same order and both comparably contribute to τ_s. As the electric field dependence of electron life time in GaAs[46] is weaker than that of spin relaxation time predicted[34], the E dependence of τ_s^r is expected to dominate the change of τ_s. We re-emphasize here that our spin-Hall angle determination from experimental results only requires τ_s that the Hanle measurements can determine.

D. Parameters for analysis in the un-doped GaAs measurements

The total electron density n_e in un-doped GaAs sample (n_e^0= 5.30×10^{14}) under the light intensity I_i=20, 40, 60, 80 mW were n_e=1.25, 1.88, 2.67, 3.28 ×10^{15} cm^{-3} respectively. In the calculation of spin polarization in un-doped GaAs, we assume that both the initial spin polarization rate P_0 and the absorption coefficient α are the same as in n-GaAs, because these are mainly determined by the wave functions and not by the doping density[45]. For I_i=20, 40, 60, 80 mW, we obtained G as 0.78, 1.57, 2.35, 3.14×10^{24} cm^{-3} respectively. Using these values in the spin density rate equation, we obtained the $E_{||}$ dependence of P and θ_{SH} in Figs. 5e and 5f. We neglect the contribution from spin-polarized holes, because hole spins relax much faster (100 fs[47]) than electron spins, although the same number of electrons and holes are optically excited.

Acknowledgment

N.O. would like to thank Funai Foundation for Information Technology, the Overseas Scholarship. H.K. acknowledges support from the Japan Science and Technology Agency (JST). T.J. acknowledges support from the EU European Research Council (ERC) advanced grant no. 268066, from the Grant Agency of the Czech Republic grant no. 14-37427G, and from the Academy of Sciences of the Czech Republic Praemium Academiae. J. S. acknowledges support from US grants ONR-N000141110780, NSF-DMR-1105512 and from the Alexander Von Humboldt Foundation. Also this project is supported by EPSRC under Grant No. EP/J003638/1.

Author contributions

N.O. designed the experimental set-up, collected and analyzed all of the data with supports of H.K., T.T., E.S. and C.H.W.B.; I.F. and D.A.R supplied the samples; J.S., J.M., T.J. provided the theory calculations; H.K., N.O., J.S. and T.J. wrote the manuscript; All authors discussed the results and commented on the manuscript.

* Electronic address: h.kurebayashi@ucl.ac.uk

[1] Kato, Y. K., Myers, R. C., Gossard, A. C. & Awschalom, D. D. Observation of the spin Hall effect in semiconductors. *Science* **306**, 1910 (2004).

[2] Wunderlich, J., Kaestner, B., Sinova, J. & Jungwirth, T. Experimental observation of the spin-Hall effect in a two dimensional spin-orbit coupled semiconductor system. *Phys. Rev. Lett.* **94**, 047204 (2005).

[3] Dyakonov, M. I. & Perel, V. I. Current-induced spin orientation of electrons in semiconductors. *Phys. Lett. A* **35**, 459 (1971); Dyakonov, M. I. & Perel, V. I. Possibility of orienting electron spins with current. *JETP Lett.* **13**, 467 (1971).

[4] Hirsch, J. E. Spin Hall Effect. *Phys. Rev. Lett.* **83**, 1834 (1999).

[5] Sinova, J. *et al.* Universal intrinsic spin-Hall effect. *Phys. Rev. Lett.* **92**, 126603 (2004).

[6] Murakami, S., Nagaosa, N. & Zhang, S-C. Dissipationless quantum spin current at room temperature. *Science* 301, 1348 (2003).

[7] Jungwirth, T., Wunderlich, J., & Olejnik. K. Spin Hall effect devices. *Nature Mater.* **11**, 382 (2012).

[8] Valenzuela, S. O. & Tinkham, M. Direct electronic measurement of the spin Hall effect. *Nature* **442**, 176 (2006).

[9] Saitoh, E., Ueda, M., Miyajima, H. & Tatara, G. Conversion of spin current into charge current at room temperature: Inverse spin-Hall effect. *Appl. Phys. Lett.* **88**, 182509 (2006).

[10] Kimura, T., Otani, Y., Sato, T., Takahashi, S. & Maekawa, S. Room-Temperature Reversible Spin Hall Effect. *Phys. Rev. Lett.* **98**, 156601 (2007).

[11] Ando, K., et al., Electrically tunable spin injector free from the impedance mismatch problem. *Nat. Mater.* **10**, 655 (2011).

[12] Matsuzaka, S., Ohno, Y. & Ohno, H. Electron density dependence of the spin Hall effect in GaAs probed by scanning Kerr rotation microscopy. *Phys. Rev. B* **80**, 241305 (2009).

[13] Garlid, E. S., Hu, Q. O., Chan, M. K., Palmstrom, C. J. & Crowell. P. A. Electrical Measurement of the Direct Spin Hall Effect in Fe/$In_xGa_{1-x}As$ Heterostructures. *Phys. Rev. Lett.* **105**, 156602 (2010).

[14] Liu, L., Buhrman, R. A., & Ralph, D. C. Review and Analysis of Measurements of the Spin

Hall Effect in Platinum. arXiv: 1111.3702.

[15] Mosendz, O.*et al.* Detection and quantification of inverse spin Hall effect from spin pumping in permalloy/normal metal bilayers. *Phys. Rev. B* **82**, 214403 (2010).

[16] Liu, L., Pai, C.-F., Li, Y., Tseng, H.W., Ralph, D.C., Buhrman, R.A. Spin-torque switching with the giant spin hall effect of tantalum. *Science* **336**, 555 (2012).

[17] Niimi, Y. et al. Extrinsic spin hall effect induced by iridium impurities in copper. *Phys. Rev. Lett.* **106**, 126601 (2011);

[18] Niimi, Y. et al. Giant Spin Hall Effect Induced by Skew Scattering from Bismuth Impurities inside Thin Film CuBi Alloys. *Phys. Rev. Lett.* **109**, 156602 (2012).

[19] Pai, C.-F., Liu, L.,, Li, Y., Tseng, H.W., Ralph, D.C., Buhrman, R.A. Spin transfer torque devices utilizing the giant spin Hall effect of tungsten. *Appl. Phys. Lett.* **101**, 122404 (2012).

[20] Gunn, J. B. Microwave oscillations of current in III-V semiconductors. *Solid State Commun.* **1**, 88 (1963).

Butcher, P. N. The Gunn effect. *Rep. Prog. Phys.* **30**, 97 (1967).

[21] Meier, F. & Zakharchenya, B. P. *Optical Orientation* (North-Holland, Amsterdam 1984).

[22] Miah, M. I. Observation of the anomalous Hall effect in GaAs. J. Phys. D: Appl. Phys. 40, 16591663 (2007).

[23] Wunderlich, J., Irvine, A. C., Sinova, J., Park, B. G., Zarbo, L. P., Xu, X. L., Kaestner, B., Novak, V., & Jungwirth T. Spin-injection Hall effect in a planar photovoltaic cell Nature Phys. **5**, 675 (2009).

[24] Wunderlich, J., Park, B. G., Irvine, A. C., Zarbo, L. P. , Rozkotova, E., Nemec, P., Novak, V., Sinova, J., & Jungwirth, T. Spin Hall effect transistor. Science **330**, 1801 (2010).

[25] Okamoto, N., Kurebayashi, H., Harii, K., Kajiwara, K., Beere, H., Farrer, I., Trypiniotis, T., Ando, K., Ritchie, D. A., Barnes, C. H. W., and Saitoh, E. Spin current depolarization under high electric fields in undoped InGaAs. Appl. Phys. Lett. **98**, 242104 (2011).

[26] Lei, X. L., Xing, D. Y., Liu, M., Ting, C. S. & Birman, J. L. Nonlinear electronic transport in semiconductor systems with two types of carriers: Application to GaAs. *Phys. Rev. B* **36**, 9134 (1987).

[27] McCumber, D.E. & Chynoweth, A.G. Theory of negative-conductance amplification and of Gunn instabilities in "two-valley" semiconductors. *IEEE Trans. Electron Devices* **ED-13**, 4 (1966).

[28] Moss, T. S. Optical Absorption Edge in GaAs and Its Dependence on Electric Field. *J. Appl. Phys.* **32**, 2136 (1961).

[29] Hubner, J., *et al.*, Temperature-dependent electron Lande g factor and the interband matrix element of GaAs. *Physical Review B* **79** 193307 (2009).

[30] Shen, K., Weng, M. Q. & Wu, M. W. *L*-valley electron *g*-factor in bulk GaAs and AlAs. *J. Appl. Phys.* **104**, 063719 (2008).

[31] Kikkawa, J. M. & Awschalom, D. D. Resonant spin amplification in *n*-type GaAs. *Phys. Rev. Lett.* **80**, 4313 (1998).

[32] Jiang, J. H. & Wu, M. W. Electron-spin relaxation in bulk III-V semiconductors from a fully microscopic kinetic spin Bloch equation approach. *Phys. Rev. B* **79**, 125206 (2009).

[33] Zhang, T. T., *et al.*, L-valley electron spin dynamics in GaAs. *Physical Review B* **87** 041201(R) (2013).

[34] Tong, H. & Wu, M. W. Multivalley spin relaxation in *n*-type bulk GaAs in the presence of high electric fields. *Phys. Rev. B* **85**, 075203 (2012).

[35] Engel, H.-A., Halperin, B. I. & Rashba, E. I. Theory of spin Hall conductivity in *n*-doped GaAs. *Phys. Rev. Lett.* **95**, 166605 (2005).

[36] Qi, Y., Yu, Z.-G., and Flatte, M. E. Spin Gunn Effect *Phys. Rev. Lett.* **96**, 026602 (2006).

[37] Jancu, J.-M., Scholz, R., Beltram, F. & Bassani, F. Empirical spds* tight-binding calculation for cubic semiconductors: General method and material parameters. *Phys. Rev. B* **57**, 6493 (1998).

[38] Sinitsyn, N. A., Hankiewicz, E. M., Teizer, W. & Sinova, J. Spin Hall and spin-diagonal conductivity in the presence of Rashba and Dresselhaus spin-orbit coupling. *Phys. Rev. B* **70**, 081312(R) (2004).

[39] Sinova, J., & MacDonald, A. H.,Theory of Spin-Orbit effects in Semiconductors, in Spintronics included in the series of Semicondcutors and Semimetals, edited by T. Dielt, D. Awschalom, M. Kaminska, and H. Ohno, Elesvier, New York (2008).

[40] Geller, C. B., Wolf, W., Picozzi, S., Continenza, A., Asahi, R., Mannstadt, W., Freeman, A. J. & Wimmer, E. Computational band-structure engineering of III-V semiconductor alloys. *Appl. Phys. Lett.* **79**, 368 (2001).

[41] Jain, A., et al., Crossover from Spin Accumulation into Interface States to Spin Injection in the Germanium Conduction Band. *Phys. Rev. Lett.* **109**, 106603 (2012).

[42] Rojas-Sanchez, J.-C, et al., Spin pumping and inverse spin Hall effect in germanium. *Phys. Rev. B* **88**, 064403 (2013).

[43] Baca, A. G., Ren, F., Zolper, J. C., Briggs, R. D. & Pearton,S. J. A survey of ohmic contacts to III-V compound semiconductors. *Thin Solid Films* **308**, 599 (1997).

[44] Ando, K. & Saitoh, E. et al. Observation of the inverse spin Hall effect in silicon. Nat. Commun. **3**, 629(2012).

[45] Casey, H. C., Sell, D. D. & Wecht, K. W. Concentration dependence of the absorption coefficient for *n*- and *p*-type GaAs between 1.3 and 1.6 eV. *J. Appl. Phys.* **46**, 250 (1975); Sell, D. D., Casey, H. C. & Wecht, K. W. Concentration dependence of the refractive index for *n*- and *p*-type GaAs between 1.2 and 1.8 eV. *J. Appl. Phys.* **45**, 2650 (1974).

[46] Rogalla, M., et al. Carrier lifetime under low and high electric field conditions in semi-insulating GaAs. Nucl. Instrum. Methods Phys. Res. A **@410**, 74 (1998).

[47] Hilton, D. J. & Tang, C. L. Optical Orientation and Femtosecond Relaxation of Spin-Polarized Holes in GaAs. *Phys. Rev. Lett.* **89**, 146601 (2002).

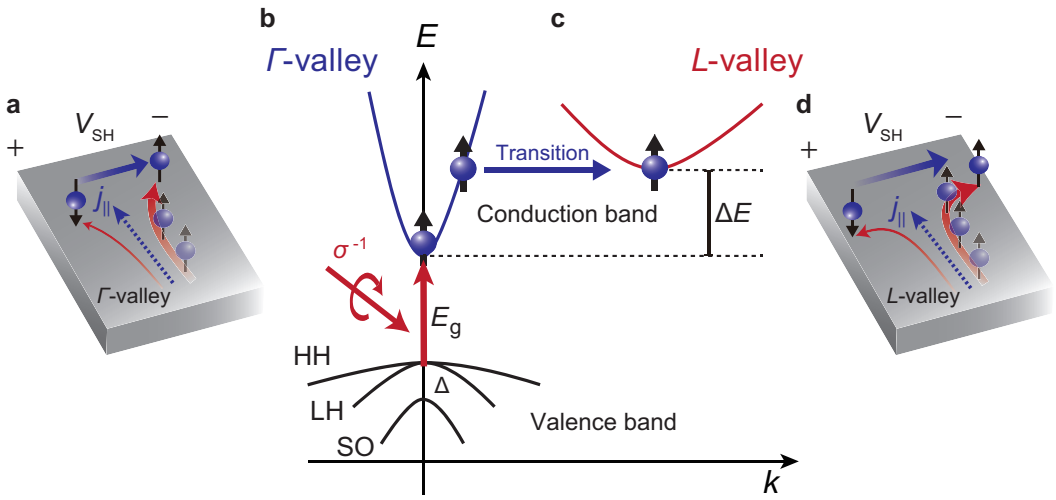

FIG. 1: Schematics of optically-induced inter-valley spin-Hall effect (SHE). **a)** The optically-induced SHE for Γ-valley electrons. **b)** GaAs band structures and spin-polarized electrons generated by circularly polarized light absorption. **c)** A high electric field induces the transition of the spin polarized electrons from the Γ-valley to the satellite L valley where part of its p-character provides a larger effective spin-orbit coupling (SOC). **d**) The optically-induced SHE for L-valley electrons. Due to the larger SOC of the L-valley electron, the magnitude of the charge-spin conversion efficiency is strongly enhanced.

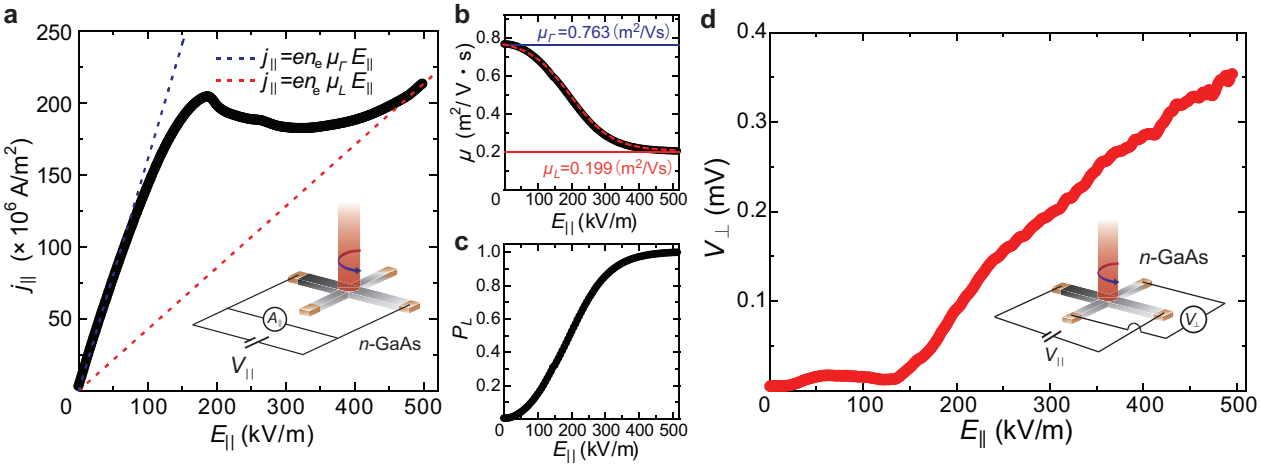

FIG. 2: Electric field dependence of the longitudinal carrier transport and optically-induced SHE voltages. **a**) Electric field $E_{||}$ dependence of the longitudinal current density $j_{||}$ in a Si-doped GaAs layer with the light excitation ($h\nu$=1.58 eV, light intensity $I_{\rm i}$=80 mW). Two dash lines represent the calculated transport characteristic purely for electrons in the Γ or L valley. The fact that the experimental data for the very high E region are on the red line suggests that electrons are fully populated in the L valley for the electric fields. **b**) Electric field $E_{||}$ dependence of the total electron mobility μ. By using the effective-mass approximation, we obtained that the mobility of the Γ-valley electron μ_Γ=0.763±0.002 m^2/Vs and of L-valley electron μ_L=0.199±0.001 m^2/Vs(see Supplementary Information for more details). The red curve is the fitting result.**c**, Electric field $E_{||}$ dependence of the electron transition rate P_L from Γ-valley to L-valley, calculated by the equation $\mu = (1-P_L)\,\mu_\Gamma + P_L\mu_L$. **d**) The optically-induced SHE voltage as a function of $E_{||}$ in the GaAs layer. We have corrected for any spin-independent components by subtracting the signal for linear polarization.

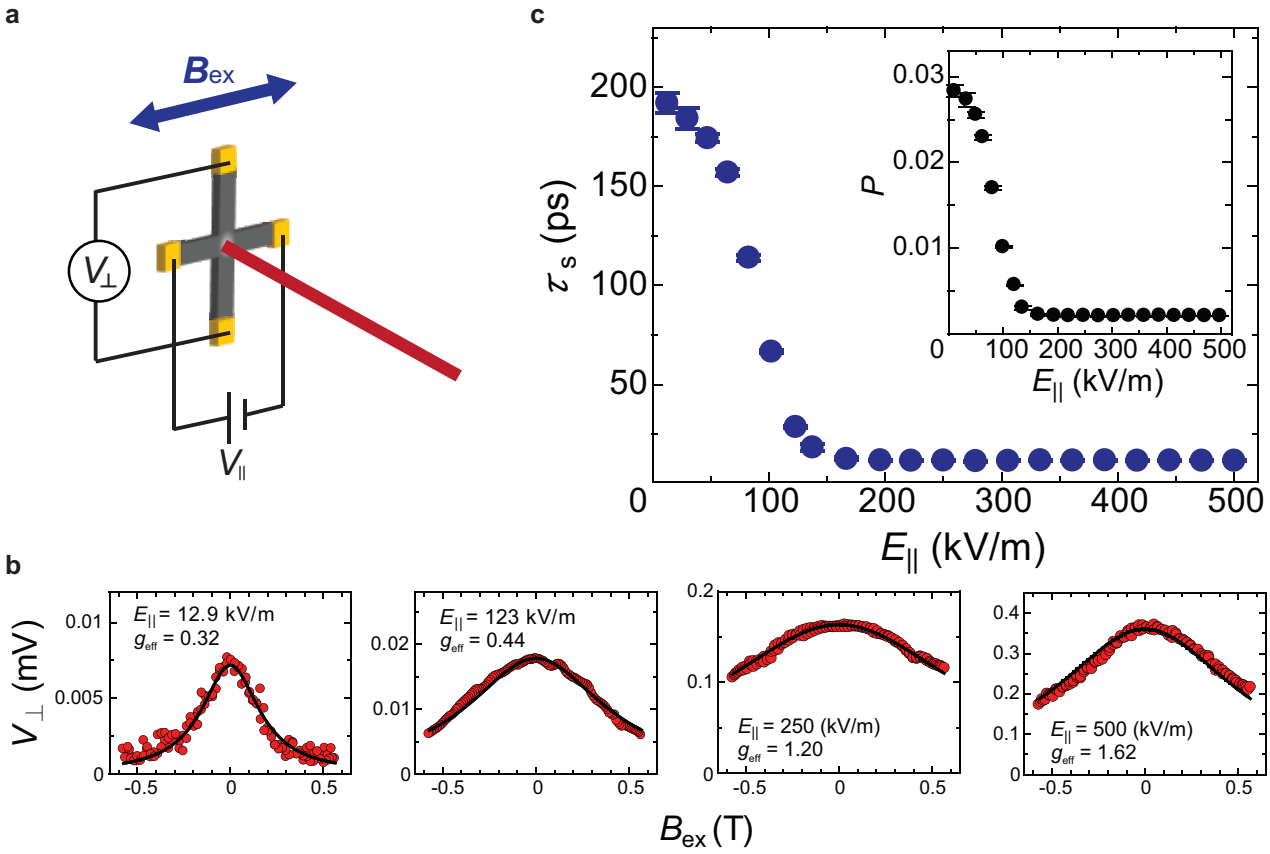

FIG. 3: Electric field dependence of Hanle effect measurement and spin polarization P in the Si-doped GaAs. **a**) A schematic of the Hanle effect measurement. During the optically-induced SHE measurements, an external magnetic field $B_{\rm ex}$ was applied along $E_{||}$ to precess the electron spins and also to avoid the influence of the normal Hall effect. **b**) Observed Hanle signals (red symbols) as a function of $B_{\rm ex}$ at $E_{||}$=12.5, 123, 250, and 500 kV/m. The solid curves are from the best-fit results with $V_{\perp}(B_{\rm ex}) = V_{\perp}(0)/\left\{1+(\Omega\tau_{\rm s})^2\right\}$, where $\tau_{\rm s}$ is spin life time and $\Omega = \mu_{\rm B} g_{\rm eff} B_{\rm ex}/\hbar$ is the Larmor frequency spin precession ($\mu_{\rm B}$, the Bohr magneton, $g_{\rm eff}$: the effective electron g-factor). **c**) Electric field dependence of $\tau_{\rm s}$ obtained from each Hanle curve. P shown in the inset was calculated from the spin density rate equation ($P = GP_0^{\rm L}\tau_{\rm s}/n_{\rm e}$) with $\tau_{\rm s}$, the initial spin polarization rate P_0, the rate of the optically excited electron density G and the total electron density $n_{\rm e}$. $\tau_{\rm s}$ and P data plots include error bars.

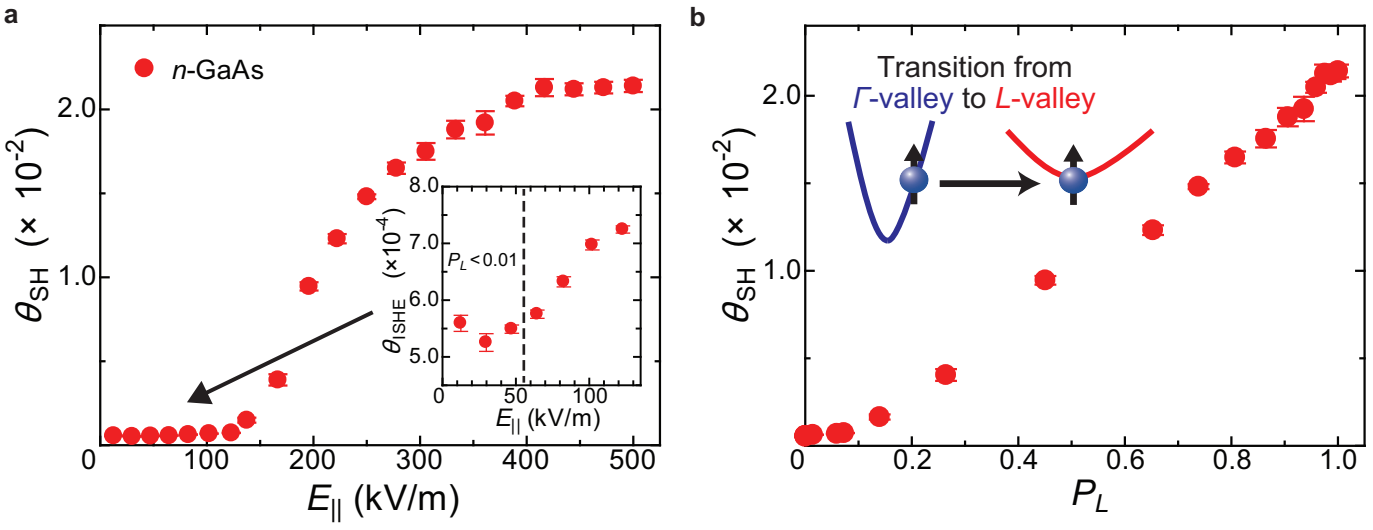

FIG. 4: Evolution of the spin-Hall angle $\theta_{\rm SH}$ in the inter-valley electron transition. **a**) Electric field $E_{||}$ dependence of the spin-Hall angle $\theta_{\rm SH}$ in the Si-doped GaAs. $\theta_{\rm SH}$ was obtained from the optically-induced SHE voltage $V_{\perp}$ and the spin polarization P. The inset shows the lower bias region. **b**) The Γ-L transition rate dependence of $\theta_{\rm SH}$. All the plots include error bars.

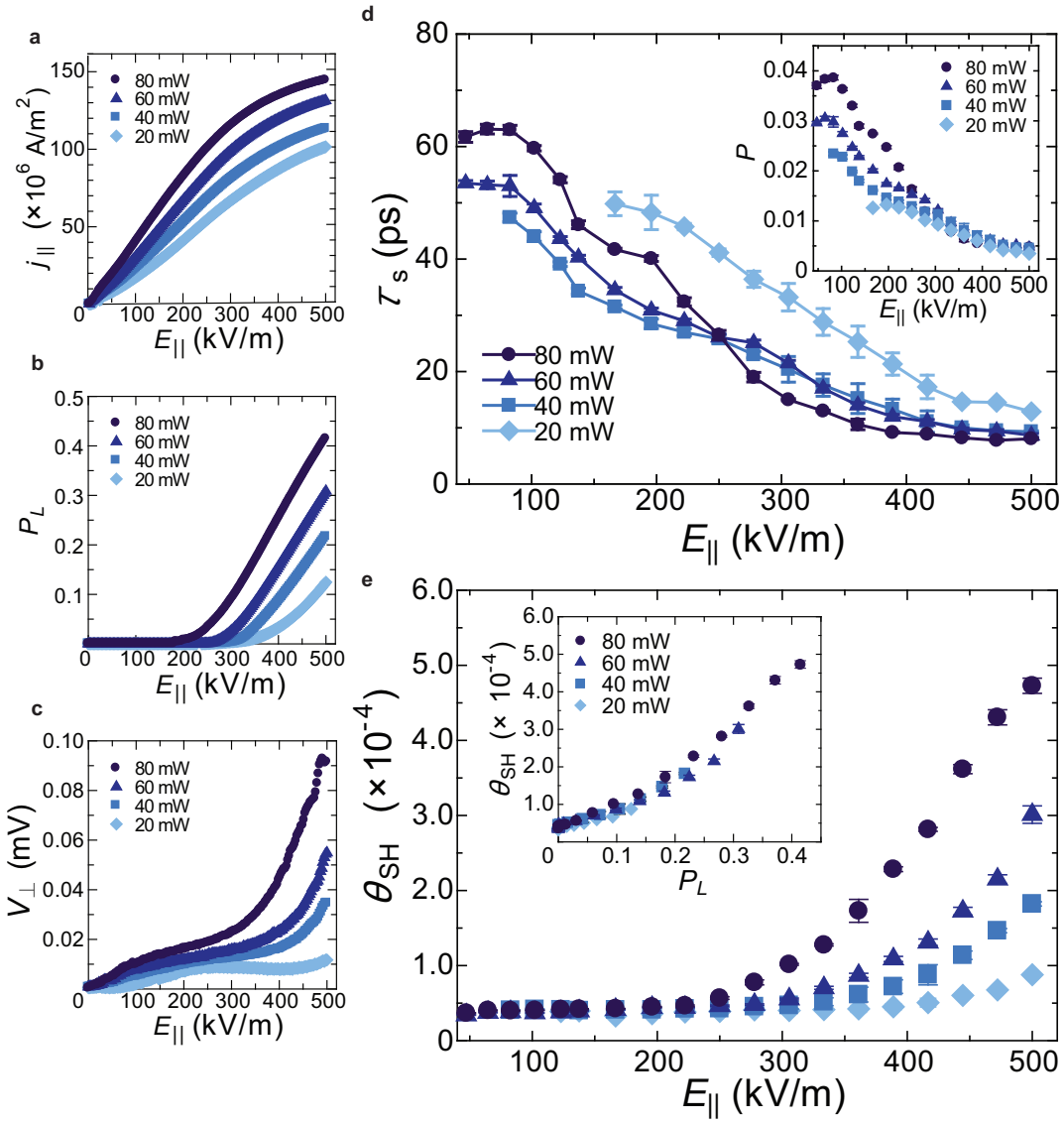

FIG. 5: Transport and optically-induced SHE voltage measurements for an un-doped GaAs. We used different light intensities: $I_{\rm i}$=20 (rhombic symbols), 40 (square symbols), 60 (triangle symbols), 80 (circle symbols) mW. **a**) Electric field $E_{||}$ dependence of the longitudinal current density $j_{||}$ with the light excitation ($h\nu$=1.58 eV). **b**) Electric field $E_{||}$ dependence of the Γ-L inter-valley transition rate P_L. **c**) The optically-induced SHE voltage as a function of the longitudinal electric field $E_{||}$. We have corrected for any spin-independent components by subtracting the signal for linear polarization. **d**) The electric field dependence of spin life time $\tau_{\rm s}$ and spin polarization P. **e**) The electric field $E_{||}$ dependence of the spin-Hall angle $\theta_{\rm SH}$. We obtained $\theta_{\rm SH}$ from $V_\perp$ and P. The inset shows $\theta_{\rm SH}$ as a function of P_L. Observe that $\theta_{\rm SH}$ excellently scales with P_L for all the light intensities measured. $\tau_{\rm s}$, P and θ plots include error bars.